J Mater Sci (2012) 47:6784–6791
DOI 10.1007/s10853-012-6619-4

Role of Mg dopant on the electrochemical performance of $LiNi_{0.5}Co_{0.5}O_2$ cathode materials for lithium rechargeable batteries

C. Nithya · S. Bharathi Devi · S. Gopukumar

Received: 11 March 2012 / Accepted: 26 May 2012 / Published online: 16 June 2012

Abstract Positive electrode materials, $LiMg_xNi_{0.5-x}Co_{0.5}O_2$ ($x = 0 < x < 0.5$), have been successfully synthesized by microwave-assisted solution technique. The precursor has been analyzed by TG/DTA and the powder was calcined at 850 °C. The XRD patterns reveal that the synthesized materials exhibit hexagonal layered structure corresponding to $R\bar{3}m$ space group. Coin cells of 2016 type have been fabricated using the synthesized layered material as cathode active material and lithium foil used as counter and reference electrode. Test cells were operated in the potential limits between 2.7 and 4.3 V using 1 M $LiPF_6$ in 1:1 EC/DEC as electrolyte. $LiMg_{0.2}Ni_{0.3}Co_{0.5}O_2$ material delivers an average discharge capacity of around 165 mA hg^{-1} at 0.1 C rate over the investigated 20 cycles.

Introduction

Lithium-ion batteries have long been considered as a suitable power source for portable electronic devices, electric vehicle, and hybrid electric vehicles (HEV) due to their high working voltage, high power density, and long cycle life [1, 2]. Nowadays, $LiMO_2$ (M = Co, Ni, Mn), $LiMPO_4$ (Fe, Co, Ni, Mn), and $LiMn_2O_4$ cathode materials are widely used as cathode materials for lithium ion batteries. Among the cathode materials, $LiCoO_2$ is the most attractive cathode (positive electrode) material because it has the theoretical capacity of 273 mA hg^{-1}. $LiCoO_2$ is the widely used cathode material in commercial lithium-ion batteries because it has many advantages such as high specific energy, high discharge capacity, high power density, low self–discharge rate, and good reversibility during charge and discharge [3–6]; however, the practical capacity of $LiCoO_2$ is limited to about 140 mA hg^{-1} i.e., around half of its theoretical capacity (273 mA hg^{-1}) [7–9]. The main disadvantage of $LiCoO_2$ is the specific capacity which decreases significantly when the material is cycled above 4.2 V, this is because extracting more Li ions than $Li_{0.5}CoO_2$ leads to a decrease in the lattice constant, transition from hexagonal to monoclinic phase, and thereby collapses the structure [10]. To improve the cycling stability of $LiCoO_2$, different attempts made to involve doping or coating with some inactive materials [11–15] have been investigated. Coating with oxides of Al, Mg, and Sn improves the cycling performance of $LiCoO_2$ [16–19]. These coating materials form a solid solution at the surface and provide a pathway for Li intercalation/deintercalation as they act as buffer to phase transition. $LiNi_{1-x}Co_xO_2$ has drawn much attention from many research groups owing to the improved electrochemical properties with higher capacity and better cycleability. The existence of Co is one of the key factors to stabilize the crystal structure of $LiNi_{1-x}Co_xO_2$ [20]. Among them $LiNi_{0.5}Co_{0.5}O_2$ is more attractive and is used as cathode material for lithium rechargeable batteries as reported by many researchers [21–23]. This material is expected to be structurally and thermally much more stable than any other nickel-rich cathode materials, especially after several cycling which provides 150 mA hg^{-1} capacity at a cutoff voltage of 4.3 V [24, 25]. Mladenor et al. [26] have reported that magnesium doping

C. Nithya · S. Gopukumar (✉)
Central Electrochemical Research Institute (CSIR–CECRI), Karaikudi 630 006, India
e-mail: deepika_41@rediffmail.com

S. B. Devi
P.G. and Research Department of Chemistry, Thiagarajar College, Madurai 625 009, India

improves both the cycling stability and the discharge capacity of $LiCoO_2$ material. In this paper, we investigate the structural and electrochemical properties of Mg-doped $LiNi_{0.5}Co_{0.5}O_2$ synthesized by microwave-assisted solution technique.

Experimental

For the synthesis of $LiMg_xNi_{0.5-x}Co_{0.5}O_2$, the stoichiometric amount of anhydrous $LiNO_3$, $Ni(NO_3)_2{\cdot}6H_2O$, $Co(NO_3)_2{\cdot}6H_2O$, and $Mg(NO_3)_2{\cdot}6H_2O$ were mixed and

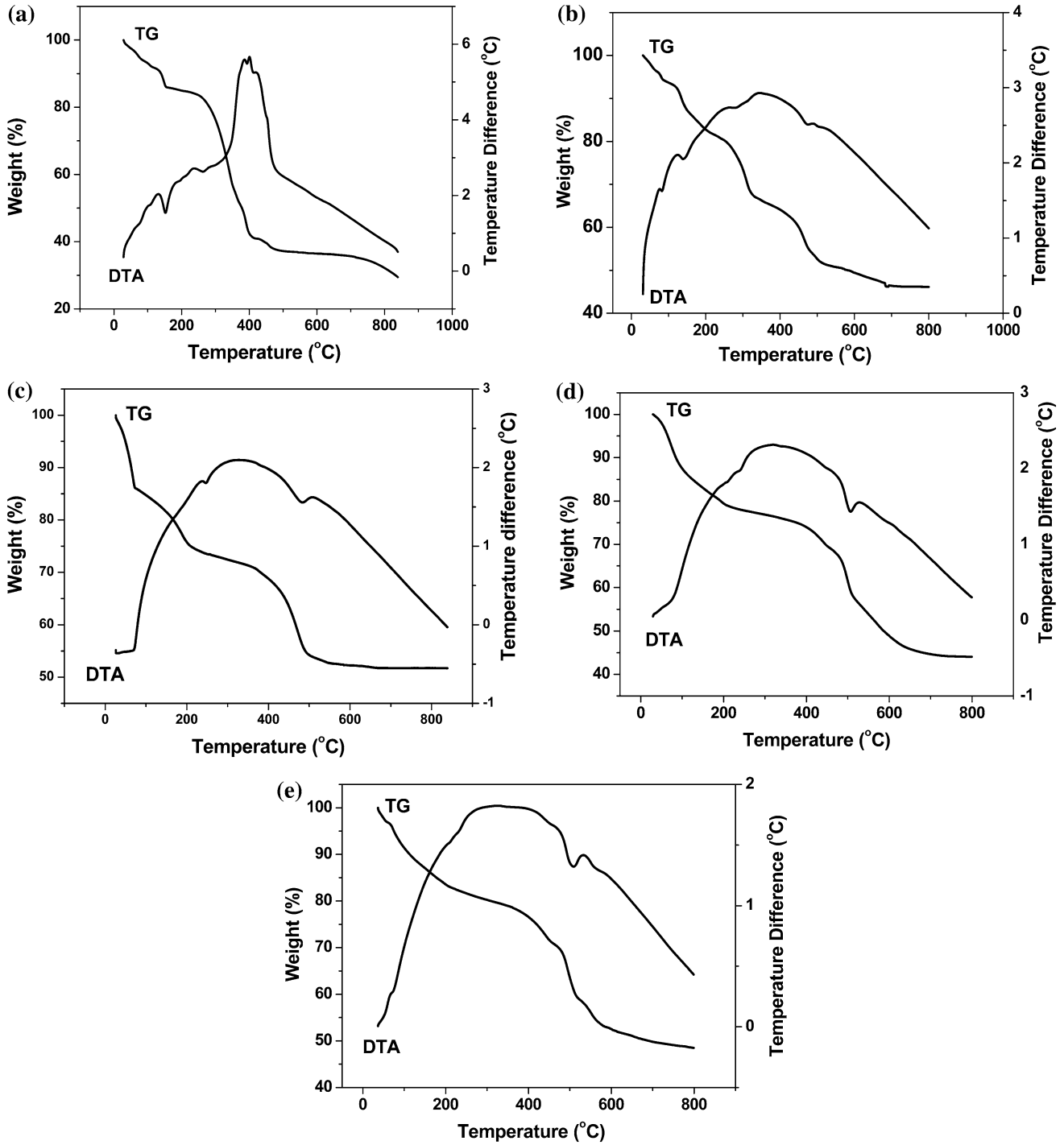

Fig. 1 TG/DTA curves of **a** $LiCoO_2$, **b** $LiNi_{0.5}Co_{0.5}O_2$, **c** $LiMg_{0.1}Ni_{0.4}Co_{0.5}O_2$, **d** $LiMg_{0.2}Ni_{0.3}Co_{0.5}O_2$, and **e** $LiMg_{0.25}Ni_{0.25}Co_{0.5}O_2$

dissolved in minimum amount of distilled water. The resulting metal ion solution was concentrated by stirring continuously under slightly warmed condition (100 °C). The above concentrated solution was transferred to china dish and placed at the center of a rotating plate of microwave oven (ken star, India 2450 MHz, 800 W) which is kept in closed chamber. The evolving NO_x gases from the reaction chamber are passed into water to avoid the hazardous nature of the gases. It is converted into nitric acid while reacting with water. The reactions are as follows:

$$3NO_2 + H_2O \rightarrow 2HNO_3 + NO$$

$$NO + NO_2 + H_2O \rightarrow 2HNO_2$$

$$4NO_2 + 2H_2O + O_2 \rightarrow 4HNO_3$$

The solution was irradiated (50 % power) for 15 min. After completion of the reaction, the product was dried in an air oven for 2 h. The resulting product was ground well and then calcined at 850 °C for 2 h in air to obtain phase pure $LiMg_xNi_{0.5-x}Co_{0.5}O_2$.

The thermal decomposition behavior of the precursor was examined by thermogravimetric analysis and differential thermal analysis in oxygen flow from 0 to 850 °C with the heating rate of 10 °C/min. The calcined product was characterized by means of XRD ('Xpert PRO PANalytical PW 3040/60 'X'Pert PRO') using Cu-Kα radiation ($\lambda = 1.5418$ Å), while the voltage and current were held at 40 kV and 20 mA ($2\theta = 0$–$80°$) at a scan rate of 1° min^{-1}. The surface morphology and microstructure of powder particles were characterized by scanning electron Microscope (SEM HITACHI S—3000 H from Japan). Fourier Transform infrared spectrum was recorded on Nicolet 5DX–FTIR Spectroscopy using KBr pellet method in the range of 400–4000 cm^{-1}.

The cathode disk was prepared by mixing 80 wt% active material, 10 wt% acetylene black, and 10 wt% polyvinylidene fluoride (PVDF) binder in *N*-methylpyrrolidone (NMP) solvent to form homogeneous slurry. The slurry mixture was coated on to an aluminum foil and dried under ambient condition and cut into circular disks of 18 mm diameter. The cut disks were further dried under vacuum at 120 °C for 12 h. Finally, coin type cells of 2016 type were assembled in an argon-filled glove box, in which lithium was used as the counter and reference electrode, celgard 2400 as the separator, and 1 M $LiPF_6$ in 1:1 EC/DEC as the electrolyte. The charge–discharge measurements were carried out on the assembled coin cell using a programmable battery tester at C/10 rate in the potential limits between 2.7 and 4.3 V.

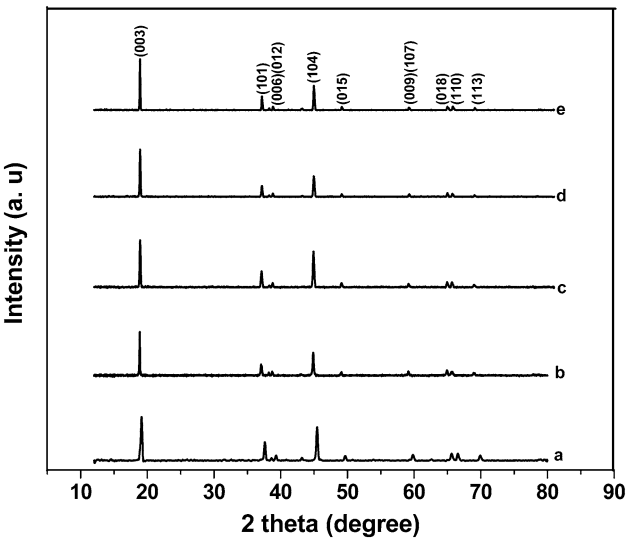

Fig. 2 XRD patterns of *a* $LiCoO_2$, *b* $LiNi_{0.5}Co_{0.5}O_2$, *c* $LiMg_{0.1}Ni_{0.4}Co_{0.5}O_2$, *d* $LiMg_{0.2}Ni_{0.3}Co_{0.5}O_2$, and *e* $LiMg_{0.25}Ni_{0.25}Co_{0.5}O_2$

Results and discussion

Thermal analysis

Figure 1a–e represent TG/DTA curves of $LiCoO_2$, $LiNi_{0.5}Co_{0.5}O_2$, and $LiMg_xNi_{0.5-x}Co_{0.5}O_2$ precursors synthesized by microwave-assisted solution technique. The thermal behavior of TG/DTA plots (Fig. 1c–e) for the precursors of $LiMg_xNi_{0.5-x}Co_{0.5}O_2$ show a similar trend.

TG curve of $LiCoO_2$ (Fig. 1a) exhibits two significant weight loss regions. In the first decomposition step (0–131 °C), there is an exothermic peak at 131 °C due to the loss of superficial water molecules, the weight loss is about 10 % in this process. At the second step (261–412 °C) (41 % weight loss), a sharp exothermic peak at 401 °C corresponds to the decomposition of nitrate precursors and can be associated with the formation of $LiCoO_2$ layered phase.

Figure 1b shows the TG/DTA curve of $LiNi_{0.5}Co_{0.5}O_2$ precursor. It can be seen from the curve that the formation of $LiNi_{0.5}Co_{0.5}O_2$ from the precursor stage can be divided into two main regions. The weight loss observed in the temperature range 0–256 °C could be ascribed to the departure of water molecules; the weight loss is about

Table 1 Unit Cell parameters for $LiMg_xNi_{0.5-x}Co_{0.5}O_2$

x	*a* (Å)	*a* (Å)	*c*/*a*	I_{003}/I_{104}	*R*	Crystallite size (nm)
$LiCoO_2$	2.818	14.014	4.973	2.49	0.53	107
0	2.845	14.069	4.945	1.80	0.48	158
0.1	2.843	14.087	4.951	1.29	0.40	87
0.2	2.851	14.095	4.943	2.33	0.35	74
0.25	2.853	14.108	4.944	2.26	0.49	133

21 % in this reaction step. The second weight loss between 325 and 515 °C (16 % weight loss), an exothermic peak at 487 °C corresponds to the formation of $LiNi_{0.5}Co_{0.5}O_2$ material.

Figure 1c–e depict the TG/DTA curves of $LiMg_xNi_{0.5-x}Co_{0.5}O_2$ precursor. TG curve shows three significant weight loss regions. The first step (0–200 °C) corresponds to the loss of superficial water molecules, 25 % weight loss in this reaction step. The second weight loss between 200 and 510 °C (5 % weight loss), an exothermic peak at 240 °C due to the decomposition of nitrate precursors. 16 % weight loss occurs between 370 and 510 °C due to metal trioxides decomposition. An exothermic peak at around 510 °C corresponds to the formation of $LiMg_xNi_{0.5-x}Co_{0.5}O_2$ phase. The presence of two endothermic peaks at 225 and 487 °C can be attributed to the melting process of metal trioxides. All the precursors show thermally inactive regions after the formation of layered phase indicating the closure of thermal events, and further heat is used to make the material more crystalline in nature.

Structural analysis

Figure 2a–e show the XRD patterns of $LiCoO_2$, $LiNi_{0.5}Co_{0.5}O_2$, and $LiMg_xNi_{0.5-x}Co_{0.5}O_2$ calcined at 850 °C. The XRD patterns are in good agreement with JCPDS card No: 44–0145. It shows single–phase formation of synthesized materials and is indexed on the basis of α-$NaFeO_2$ layered structure with $R\bar{3}m$ space group. The atoms Co, Li, and O are located in the Whyhoff sites 3a, 3b, and 6c, respectively. The synthesized layered materials are free from NiO, Co_3O_4, and $LiNO_3$ impurity phases whose intense

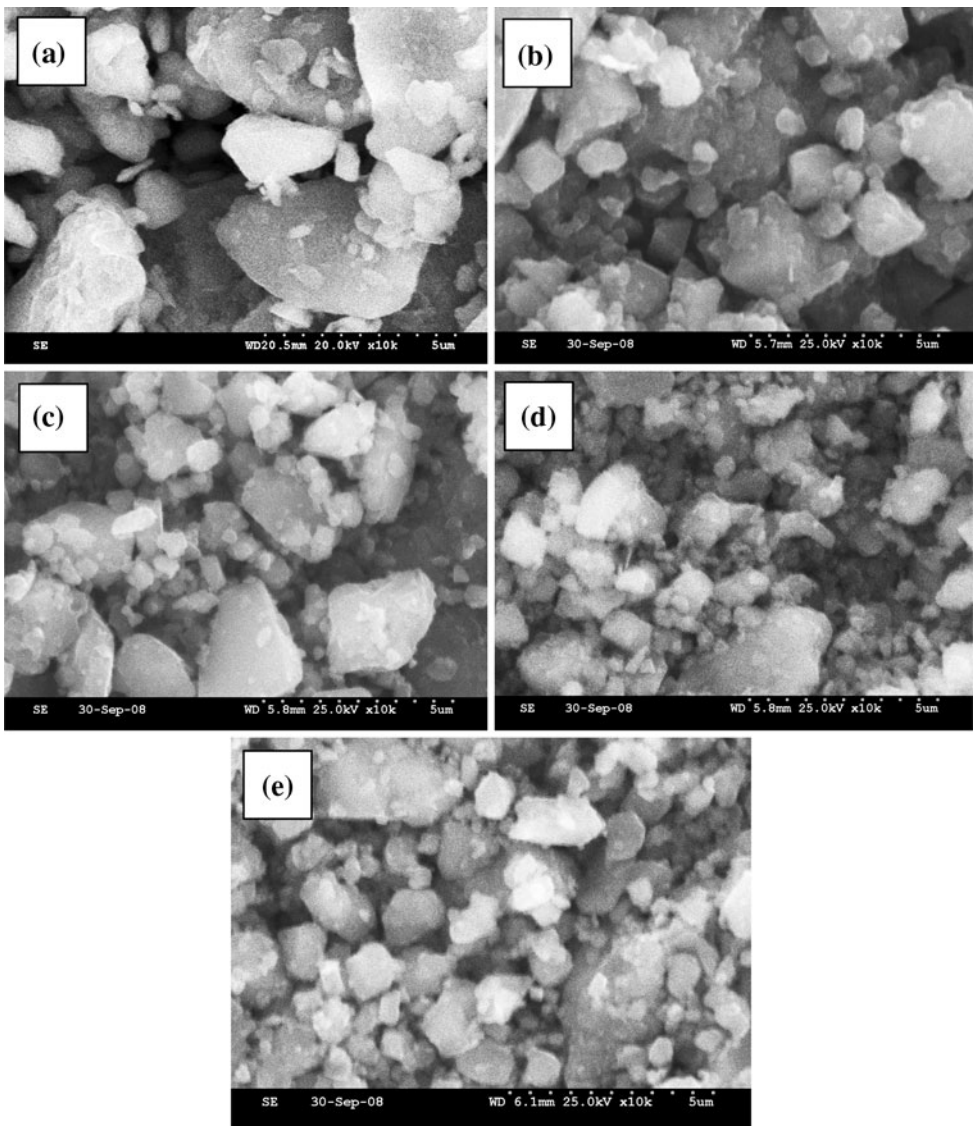

Fig. 3 SEM images of **a** $LiCoO_2$, **b** $LiNi_{0.5}Co_{0.5}O_2$, **c** $LiMg_{0.1}Ni_{0.4}Co_{0.5}O_2$, **d** $LiMg_{0.2}Ni_{0.3}Co_{0.5}O_2$, and **e** $LiMg_{0.25}Ni_{0.25}Co_{0.5}O_2$

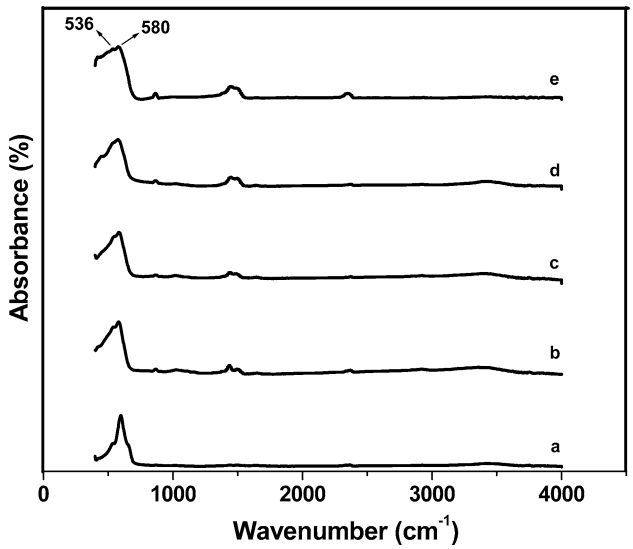

Fig. 4 FT–IR spectra of *a* $LiCoO_2$, *b* $LiNi_{0.5}Co_{0.5}O_2$, *c* $LiMg_{0.1}Ni_{0.4}Co_{0.5}O_2$, *d* $LiMg_{0.2}Ni_{0.3}Co_{0.5}O_2$, and *e* $LiMg_{0.25}Ni_{0.25}Co_{0.5}O_2$

peaks are expected at 18.012°, 33.812°, and 25.682°, respectively [25]. Furthermore, the patterns of the doped material exhibit a leftward shift in the axis of 2θ compared with $LiNi_{0.5}Co_{0.5}O_2$ because the ionic radius of Mg^{2+} (0.72 Å) is larger than Ni^{2+} (0.69 Å). The hexagonal lattice parameters of the synthesized materials are presented in Table 1 and calculated by unit cell package software with the estimated standard deviation of 0.0132. The lattice parameter 'a' does not vary much but the 'c' lattice parameter slightly increases after doping with Mg^{2+} ion because the size of the Mg^{2+} (0.72 Å) ion is larger than Ni^{2+} (0.69 Å) ion. The small lattice constants for $LiCoO_2$ may be due to the fact that decrease of electrostatic repulsion between the oxide ions across the vander walls gap as observed by Vankatraman et al. [27]. It can be noted that the ratio of the intensities of 003 and 104 (I_{003}/I_{104}) peaks is greater than unity, which suggests that there is no cation disorder, hence it is consistent with the values of c/a, i.e. >4.89. Further, as can be seen in Table 1, the c/a ratios

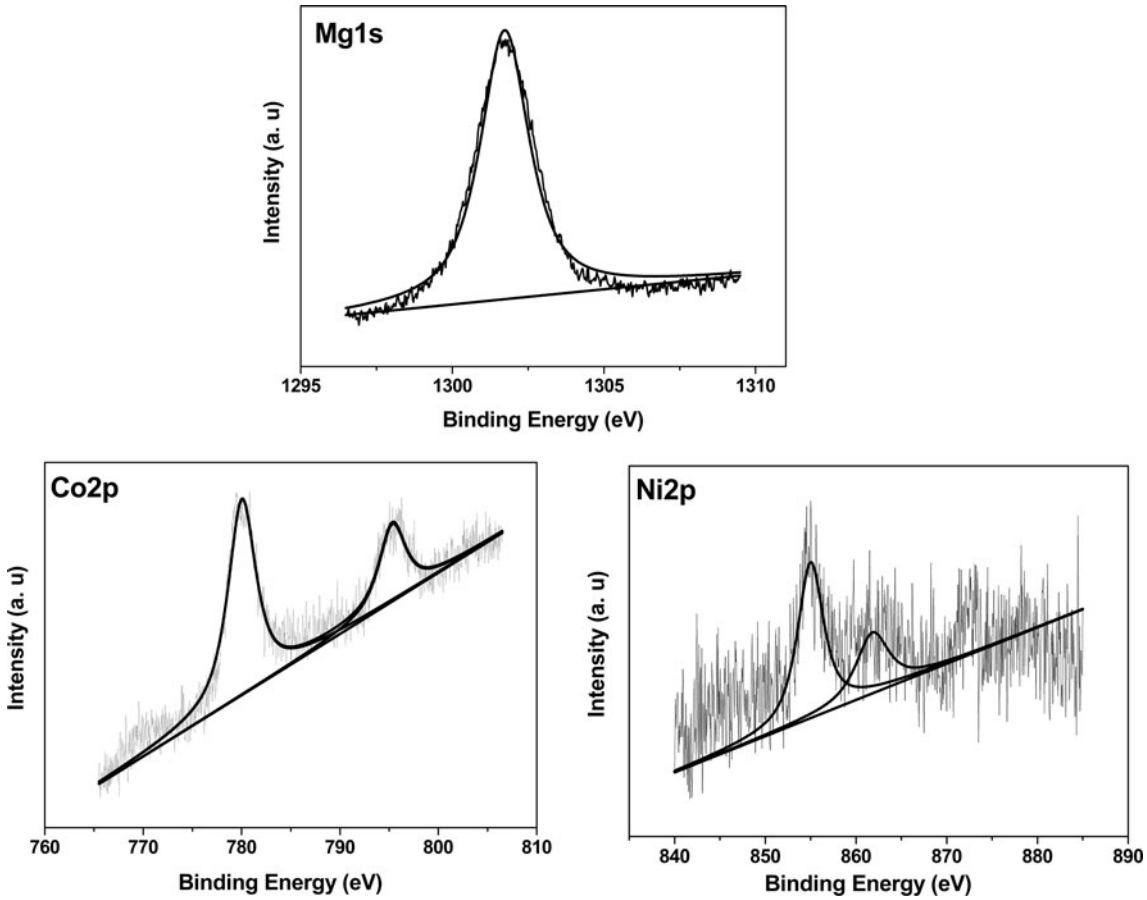

Fig. 5 XPS analysis of $LiMg_{0.2}Ni_{0.3}Co_{0.5}O_2$

are in the range of 4.95–4.97 thereby indicating no cation mixing. According to Reimers et al. [28], we observe that the 'R' factor i.e. the ratio of $(I_{006} + I_{102})/I_{101}$ are minimal for $x = 0.2$ compositions which are attributed to increased layer characteristics than $LiCoO_2$ and other dopant compositions. Crystallite sizes of the powders are calculated by Debye–Scherrer's equation and are presented in Table 1. All the results mentioned above clearly confirmed the formation of well-ordered layered structure.

Surface morphology

Scanning electron microscope images of $LiCoO_2$, $LiNi_{0.5}Co_{0.5}O_2$, and $LiMg_xNi_{0.5-x}Co_{0.5}O_2$ synthesized by microwave-assisted solution technique calcined at 850 °C are shown in Fig. 3a–e and show that the particles are inhomogeneous with serious agglomeration. As can be seen in figure, the composition with $x = 0.2$ has smaller particle size compared to other doped and undoped materials. This kind of materials should exhibit good electrochemical activity during cycling.

Vibrational spectroscopy

Figure 4a–e show the FTIR spectra of $LiCoO_2$, $LiNi_{0.5}Co_{0.5}O_2$, and $LiMg_xNi_{0.5-x}Co_{0.5}O_2$ synthesized by microwave-assisted solution technique calcined at 850 °C. The band at around 536 cm^{-1} [29] has been assigned to Li–O stretching vibration, which indicates the formation of LiO_6 octahedra. The characteristic vibrations of Co–O are 560–590 cm^{-1} [30], Ni–O and Mg–O are 579 and 630 cm^{-1}, respectively [31, 32]; but in this present work, the broad band located at around 580 cm^{-1} is attributed to the asymmetric stretching modes of MO_6 (M = Ni, Co) group. The broadening of the high-wavenumber IR bands may be related with inhomogeneous Mg/Ni/Co distribution, variation in the cation–anion bond lengths, and/or polyhedral distortion occurring in these materials [32]. It has been reported [34] that the local distortion increases with the decrease of the cobalt concentration in the solid solution.

XPS analysis

Figure 5 presents the XPS analysis of $LiMg_{0.2}Ni_{0.3}Co_{0.5}O_2$ cathode material. The binding energy observed for Mg1 s is 1302 eV which is characteristic of Mg in +2 oxidation state [35]. The Co2p binding energies observed at 780.3 and 793.9 eV correspond to $Co2p_{3/2}$ and $Co2p_{1/2}$ spin states. These ascertain that the presence of Co is in trivalent state [36]. The binding energy observed for Ni2p core level at 854.6 eV with a satellite peak of 862. 8 eV indicates that Ni is in 2+ state [37]. The observed binding energies of Ni2p and Co2p which are consistent with $LiNi_{0.5}Co_{0.5}O_2$ cathode material were reported by Zhou et al. [38]. Therefore, the missing charge in the Ni site after doping with Mg^{2+} ion is compensated by oxygen vacancies. These kinds of oxygen vacancies usually occurred in $Li_xNi_{1-x}O$ type materials, which was confirmed by XAS analysis of O1s reported by Kuiper et al. [39].

Electrochemical performance

The initial charge–discharge curves of $LiCoO_2$, $LiNi_{0.5}Co_{0.5}O_2$, and $LiMg_xNi_{0.5-x}Co_{0.5}O_2$ are shown in Fig. 6a. Test cells were operated over the voltage range of 2.7–4.3 V at 0.1 C rate. The initial discharge capacities of $LiCoO_2$, $LiNi_{0.5}Co_{0.5}O_2$, $LiMg_{0.1}Ni_{0.4}Co_{0.5}O_2$, $LiMg_{0.2}Ni_{0.3}Co_{0.5}O_2$, and $LiMg_{0.25}Ni_{0.25}Co_{0.5}O_2$ are 128, 142, 154, 170, and 162 mA hg^{-1}, respectively. The shapes of the charge–discharge curves are in good agreement with the

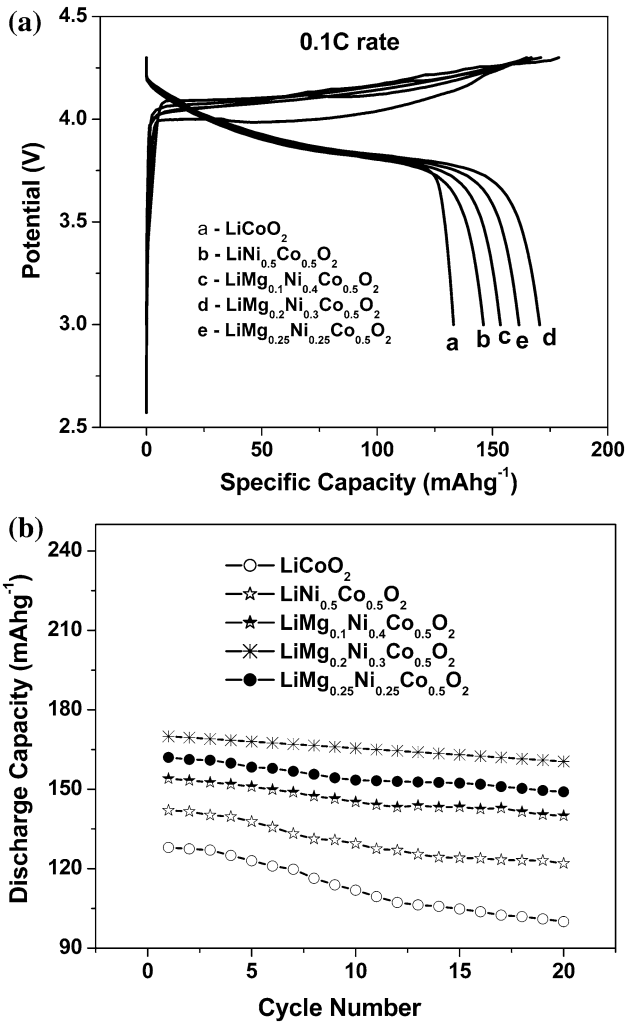

Fig. 6 Initial charge–discharge curves and cycling performance of $LiMg_xNi_{0.5-x}Co_{0.5}O_2$ cathode materials at 0.1 C rate

previous workers [40–42]. The Mg-doped materials exhibit large discharge capacity, which is attributed to the improved structural stability with the addition of dopant. The dopant prevents the dissolution of transition metal ions in the electrolyte and thwarts the collapse of the structure during charge–discharge by the limited action of Co^{4+} ions which assisted to retain its layered structure. In the case of pristine $LiCoO_2$, the over intercalation–deintercalation reaction of Li ions disintegrate the $LiCoO_2$ structure which further increases the internal impedance of the cell [43] and decreases the discharge capacity. Due to the large polarization and large change in unit cell volume during cycling in $LiNi_{0.5}Co_{0.5}O_2$ which exhibits lower discharge capacity as compared to the Mg-doped materials.

Cycling performance of the synthesized $LiMg_xNi_{0.5-x}Co_{0.5}O_2$ materials at 0.1 C rate over 20 cycles are shown in Fig. 6b. The capacity retentions of $LiCoO_2$, $LiNi_{0.5}Co_{0.5}O_2$, $LiMg_{0.1}Ni_{0.4}Co_{0.5}O_2$, $LiMg_{0.2}Ni_{0.3}Co_{0.5}O_2$, and $LiMg_{0.25}Ni_{0.25}Co_{0.5}O_2$ are 78.12, 85.91, 90.9, 94.1,and 91.9 %, respectively, after 20 cycles. The capacity retention of the $LiMg_{0.2}Ni_{0.3}Co_{0.5}O_2$ materials is larger than the material synthesized by same microwave process [25]. The dopant Mg^{2+} ion provides the cycling stability as well as structural stability which are due to pillaring effect [44, 45]. It facilitates the free movement of Li^+ ion and prevents the vacancy ordering because the dopant ion increases the 'c' lattice parameter. This enlargement of the crystal lattice provides more space for lithium ion intercalation and deintercalation which enhances the cycling stability. The obtained discharge capacities and capacity retentions are superior to $LiNi_{0.5}Co_{0.5}O_2$ cathode materials [46–49] and Al doped $LiNi_{0.5}Co_{0.5}O_2$ [50] materials.

Figure 7 presents the differential capacity curves of $LiCoO_2$, $LiNi_{0.5}Co_{0.5}O_2$, and $LiMg_{0.2}Ni_{0.3}Co_{0.5}O_2$ cathode materials which are derived from charge/discharge measurements. The anodic peak located at 3.9, 4.1, and 4.16 V corresponding cathodic peaks at 3.75, 3. 81, and 3.85 V for $LiCoO_2$, $LiNi_{0.5}Co_{0.5}O_2$, and $LiMg_{0.2}Ni_{0.3}Co_{0.5}O_2$, respectively. These are the characteristic behaviors of lithium intercalation/deintercalation process of these cathode

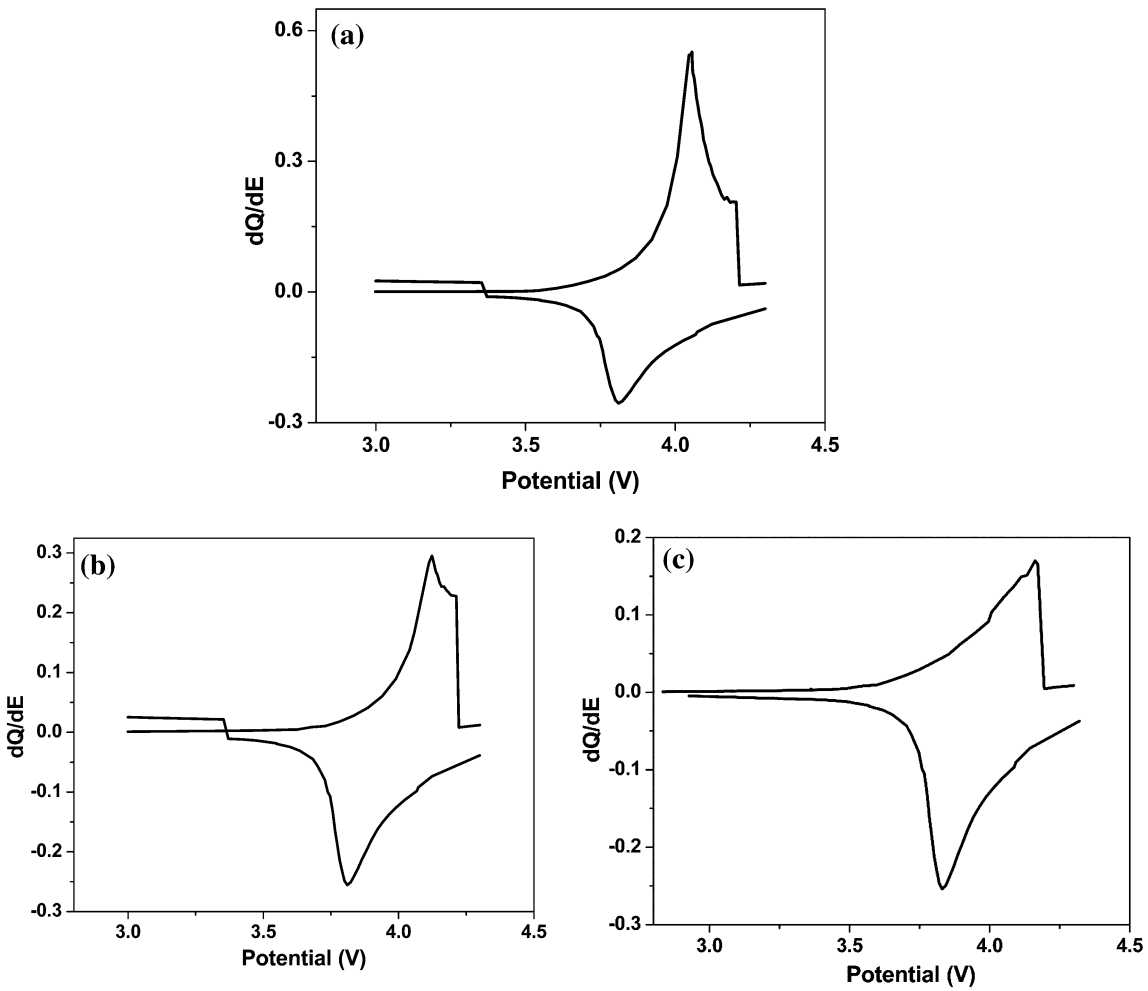

Fig. 7 Differential capacity curves of **a** $LiCoO_2$, **b** $LiNi_{0.5}Co_{0.5}O_2$, and **c** $LiMg_{0.2}Ni_{0.3}Co_{0.5}O_2$ materials at 0.1 C rate

materials. In the anodic region of $LiCoO_2$ and $LiNi_{0.5}Co_{0.5}O_2$, we observed the additional peaks at 4.16 and 4.2 V, respectively, which are due to the phase transformation of hexagonal to monoclinic [51] but it does not happen in $LiMg_{0.2}Ni_{0.3}Co_{0.5}O_2$ cathode material which is evident that the Mg^{2+} ion prevents the phase transformation during cycling. In the present work oxidations of Ni^{2+} ions and Co^{3+} ions occur at single step which is in good agreement with the previous works [52–54].

Conclusion

Layered $LiMg_xNi_{0.5-x}Co_{0.5}O_2$ was successfully synthesized by microwave-assisted solution technique. XRD patterns of $LiMg_xNi_{0.5-x}Co_{0.5}O_2$ powder showed the formation of layered structure (space group $R\bar{3}m$) and its phase purity. The synthesized material $LiMg_{0.2}Ni_{0.3}Co_{0.5}O_2$ delivers an average discharge capacity of 165 mA hg^{-1} after 20 cycles when cycled between 2.9 and 4.3 V. Charge–discharge studies confirmed that Mg doping improves the electrochemical performance of $LiNi_{0.5}Co_{0.5}O_2$ materials.

Acknowledgements The authors thank the Department of Science and Technology (DST), India for support of this work under the DST–JST project GAP12/08. One of the authors C. Nithya wishes to thank Ministry of New and Renewable Energy (MNRE), India for Senior Research Fellowship.

References

1. Weanstock IB (2002) J Power Sources 110:471
2. Bates JB, Dudney NJ, Neudecker B, Ueda A, Evans CD (2000) Solid State Ionics 135:33
3. Orman HJ, Wiseman PJ (1984) Acta Crystallogr 40:12
4. Hewston TA, Chamber Land BL (1987) J Phys Chem Solids 48:97
5. Mizushima K, Jones PC, Wise Man PC, Goodenough JB (1980) Mater Res Bull 15:783
6. Perkins JD, Bahn CS, Parilla PA, McGraw JM, Fu ML, Duncan M, Yu H, Ginley DS (1999) J Power Sources 81–82:675
7. Abraham KM, Pasquariello BM, Will Staedt EM (1998) J Electrochem Soc 145:482
8. Zhang SS, Xu K, Jow TR (2002) J Electrochem Soc 149:A1521
9. Reimers JN, Dahn JR (1992) J Electrochem Soc 139:2091
10. Anraya M, Dahn JR, Preston JS, Romen E, Reimers JN (1993) J Electrochem Soc 140:575
11. Gu Y, Chen D, Jiao X, Liu F (2007) J Mater Chem 17:1769
12. Levaneur S, Menetrier M, Suard E, Delmas C (2000) Solid State Ionics 128:11
13. Alcantara R, Lavela P, Jirado JL, Zhechera E, Stoyanova R (1999) J Solid State Electrochem 3:121
14. Kweon HJ, Kim SJ, Park DG (2000) J Power Sources 88:255
15. Tukamoto H, West AR (1997) J Electrochem Soc 144:3164
16. Kweon HJ, Park DG (2000) Electrochem Solid-State Lett 3:128
17. Cho J, Kim YJ, Pak B (2000) Chem Mater 12:3788
18. Cho J, Kim CS, Yoo SI (2000) Electrochem Solid State Lett 3:362
19. Jang Y, Huang B, Wang H, Sadoway DR, Ledar G (1999) J Electrochem Soc 146:862
20. Wang Z, Liu L, Cheng L, Huang X (2002) Solid State Ionics 148:335
21. Lui L, Wang Z, Li H, Chen L, Huang X (2002) Solid State Ionics 152–153:341
22. Myung ST, Kumagai N, Komaba S, Chung HT (2001) Solid State Ionics 139:47
23. Kim YJ, Kim TJ, Shin JW, Park B, Cho J (2002) J Electrochem Soc 49(10):A1337
24. Belharouak I, Tsukamoto H, Amine K (2003) J Power Sources 119–121:175
25. Yang S, Yue H, Yin Y, Yang J, Yang W (2006) Electrochim Acta 51:4971
26. Maldenov M, Stoya Nova R, Zhecheva E, Vassilev S (2001) Electrochem Commun 3:410
27. Vankatraman S, Manthiram A (2005) Solid State Ionics 176:291
28. Reimers JN, Rossen E, Jones CD, Dahn JR (1993) Solid State Ionics 61:335
29. Ooms FGB, Kelder EM, Schoonman J, Wagemaker M, Mulder FM (2002) Solid State Ionics 152–153/143–153
30. Andres-Verges M, Mifsud A, Serna C, Chem J (1990) J Chem Soc Faraday Trans 86:959
31. Julien C (2003) Solid State Ionics 157:57
32. Balbuena P, Wang Y (eds) (2004) Lithium-ion batteries: solid electrolyte interphase. Imperial College Press, London, p 185
33. Julien C, Letranchant C, Rangan S, Lemal M, Ziolkiewicz S, Castro-Garcia S, El -Farh L, Benkaddour M (2000) Mater Sci Eng B 76(2):145
34. Delmas C, Saadoune I (1992) Solid State Ionics 53–56:370
35. Choi YM, Pyun SI, Moon SI (1994) Solid State Ionics 89:43
36. Balbuena P, Wang Y (eds) (2004) Lithium-ion batteries: solid electrolyte interphase. Imperial College Press, London, p 185
37. Amine K, Tukamato H, Yasuda H, Fujita Y (1996) J Electrochem Soc 143:1607
38. Zhou Y, Li H (2002) J Mater Sci 37:5261. doi:10.1023/A:1021060604781
39. Kuiper P, Kruizinga G, Ghijsen J, Sawatzky GA, Verweij H (1989) Phys Rev Lett 62:221
40. Rougier A, Saadoune I, Gravereau P, Willmann P, Delmas C (1996) Solid State Ionics 90:83
41. Delmas C, Saadoune I, Rougier A (1993) J Power Sources 43–44:595
42. Levasseur S, Menetrier M, Delmas C (2002) J Power Sources 112:419
43. Julien C, Camacho-Lopez MA, Mohan T, Chitra S, Kalyani P, Gopukumar S (2000) Solid State Ionics 135:241
44. Kim HS, Ko TK, Na BK, Cho WI, Chao BW (2004) J Power Sources 138:232
45. Ohzuku T, Ueda A (1994) J Electrochem Soc 141:2972
46. Subramanian V, Karki K, Rambabu B (2004) Solid State Ionics 175:315
47. Wang GX, Horvat J, Bradhurst DH, Liu HK, Dou SX (2000) J Power Sources 85:279
48. Song M, Song J, Bang E, Mumm DR (2009) Ceram Int 35:1625
49. Kim HK, Seong YT, Yoon YS (2004) Thin Solid Films 447–448:619
50. Castro-Garcia S, Castro-Couceiro A, Rodriguez MAS, Soulette F, Julien C (2003) Solid State Ionics 156:15
51. Gopukumar S, Jeong Y, Kim KB (2003) Solid State Ionics 159:223
52. Hong YS, Park YJ, Ryu KS, Changand SH, Shin YJ (2005) J Power Sources 147:214
53. Guo J, Jiao LF, Yuan HT, Li HX, Zhangand M, Wang YM (2006) Electrochim Acta 51:3731
54. Hwang BJ, Santhanam R, Chen CH (2003) J Power Sources 114:244